Optics Letters

# Nonlinear pulse compression to 43 W GW-class few-cycle pulses at 2 μm wavelength

M. Gebhardt,[1,2,*] C. Gaida,[1] T. Heuermann,[1,2] F. Stutzki,[1,5] C. Jauregui,[1] J. Antonio-Lopez,[3] A. Schulzgen,[3] R. Amezcua-Correa,[3] J. Limpert,[1,2,4] and A. Tünnermann[1,2,4]

[1]Institute of Applied Physics, Abbe Center of Photonics, Friedrich-Schiller-Universität Jena, Albert-Einstein-Str. 15, 07745 Jena, Germany
[2]Helmholtz-Institute Jena, Fröbelstieg 3, 07743 Jena, Germany
[3]CREOL, College of Optics and Photonics, University of Central Florida, Orlando, Florida 32816, USA
[4]Fraunhofer Institute for Applied Optics and Precision Engineering, Albert-Einstein-Str. 7, 07745 Jena, Germany
[5]Current address: Fraunhofer Institute for Applied Optics and Precision Engineering, Albert-Einstein-Str. 7, 07745 Jena, Germany
*Corresponding author: martin.gebhardt@uni-jena.de

Received 24 August 2017; revised 14 September 2017; accepted 15 September 2017; posted 15 September 2017 (Doc. ID 305502); published 13 October 2017

**High-average power laser sources delivering intense few-cycle pulses in wavelength regions beyond the near infrared are promising tools for driving the next generation of high-flux strong-field experiments. In this work, we report on nonlinear pulse compression to 34.4 μJ-, 2.1-cycle pulses with 1.4 GW peak power at a central wavelength of 1.82 μm and an average power of 43 W. This performance level was enabled by the combination of a high-repetition-rate ultrafast thulium-doped fiber laser system and a gas-filled antiresonant hollow-core fiber.** 

***OCIS codes:*** (320.0320) Ultrafast optics; (320.5520) Pulse compression; (140.3070) Infrared and far-infrared lasers.

https://doi.org/10.1364/OL.42.004179

Ultrafast laser sources emitting at around 2 μm wavelength have become important tools for numerous applications in spectroscopy [1], metrology [2], and material processing [3]. More recently there has been a tremendous effort aimed at scaling the performance of these laser systems to transform them into mature drivers for strong-field experiments and nonlinear frequency conversion processes, which require considerably high peak intensities.

Such laser systems enable the generation of high-order harmonics (HHG) with high photon energy cutoff [4], owing to the fact that the ponderomotive potential scales with the square of the laser wavelength. One essential requirement for a laser to efficiently drive high cutoff HHG is to deliver few-cycle pulses, because this allows reaching high peak intensities (leading to a high conversion efficiency and a high photon energy cutoff [5]) without degrading the phase matching by undesired ionization. Furthermore, a few-cycle driver facilitates the generation of isolated attosecond pulses [6]. Resulting from the recent progress in laser development, HHG sources driven by few-cycle 2 μm laser systems have led to cutting-edge results, such as the time-resolved observation of light-induced chemical reaction paths [7] and x-ray absorption edge spectroscopy of organic molecules [4].

Similarly, high-power 2 μm laser systems with few-cycle pulse durations are extremely interesting drivers for generating ultra-broad mid-infrared (mid-IR) phase-stable frequency combs via intra-pulse difference frequency generation (DFG) [8,9]. Here, it is important to start with very short pulses coming from the driving laser to provide chirp-free frequency components with wide spectral separation, such that the generated mid-IR DFG spectra can extend to short wavelengths. With respect to the mid-IR bandwidth and power, it is very beneficial to drive the DFG at around 2 μm wavelength, as this allows using non-oxide nonlinear crystals that offer high nonlinearity, broad phase matching, and, most importantly, excellent spectral transmission up to 20 μm wavelength. A source covering the whole mid-IR with powerful, phase-stable ultrafast emission is extremely interesting for high-sensitivity and high-precision fingerprint absorption spectroscopy.

Certainly, the ever-growing number of applications that greatly benefit from intense few-cycle laser sources emitting beyond the well-explored near-IR wavelength region leads to a strongly increasing demand for these sources to deliver higher and higher average powers. In particular, the above-mentioned applications can be significantly improved (e.g., in terms of signal-to-noise ratio and data acquisition times) if higher HHG photon-flux or mid-IR power can be reached.

The traditional approach for the generation of intense few-cycle laser pulses at around 2 μm wavelength relies on nonlinear parametric amplification [10,11]. However, scaling this concept to tens of watts has so far remained challenging because of the complexity of the pump sources, as well as due to the transmission and the thermal properties of the oxide-based crystals in use. On the other hand, we have recently introduced an alternative approach that is based on nonlinear post compression of ultrashort pulses delivered by high-repetition-rate thulium-doped fiber laser systems [12,13]. To date, these laser systems are capable of generating ultrashort pulses with more than 100 W average power

[14] and a few GW pulse peak power with about 200 fs pulse duration [15]. In fact, nonlinear pulse compression (NPC) in the 2 μm wavelength region also has been investigated starting from solid-state and nonlinear parametric amplifiers [16,17]. However, as mentioned above, the available average power was limited to a few watts by the driving laser.

In this Letter, we report on nonlinear self-compression of ultrashort pulses from a thulium-doped fiber laser using a gas-filled antiresonant hollow-core fiber (ARHCF). The key features to the pulse evolution in the experiment presented herein are the broad gain bandwidth of the active medium [18], allowing for clean 110 fs pulses from the laser system itself, as well as the excellent transmission and weak anomalous dispersion of the ARHCF, leading to self-compression of the spectrally broadened pulses. We have generated 34.4-μJ pulses with a FWHM duration of only 13 fs and a pulse peak power of 1.4 GW at a central wavelength of 1.82 μm. The combination of two average power scalable concepts for the generation and the post compression of ultrashort pulses in this wavelength region is the key to high-power operation, allowing for an average power of 43 W. This is, to the best of our knowledge, the highest average power reported for any 2 μm few-cycle laser source to date.

A schematic of the experimental setup can be seen in Fig. 1. The laser source, which enabled the experiments presented herein, was a thulium-doped fiber chirped-pulse amplification system (Tm:FCPA) with an architecture similar to the one described in Ref. [15]. As compared to this earlier reported work, we have increased its spectral bandwidth to about 140 nm, which was possible thanks to an improved stretcher and compressor design, as well as the broad gain-bandwidth of thulium-doped silica. The spectrum was centered around 1920 nm wavelength, which ultimately means that detrimental propagation effects arising from the absorption lines of atmospheric water vapor have to be circumvented [19]. Regarding the thermal lens arising from water vapor absorption in a gaseous atmosphere, also described as thermal blooming, it was found that the best mitigation is to reduce the pressure of the medium in which the beam propagates [13]. Hence, the high-power sections of the laser system were enclosed in a vacuum chamber that was held at a pressure below 0.1 mbar. When adapted for the nonlinear compression experiments, the Tm:FCPA delivered 51 W of average power, corresponding to 41 μJ of pulse energy at a repetition rate of 1.25 MHz. Its output pulse duration (FWHM) was 110 fs. The measured pulse spectrum as well as an intensity autocorrelation trace are depicted in Figs. 2 and 3, respectively (black line).

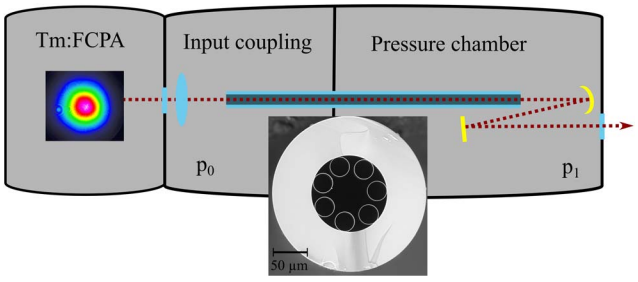


**Fig. 1.** Experimental setup for the nonlinear pulse compression experiments comprising the laser output and two separate chambers filled with gas at pressures $p_0$ and $p_1$ (connected by the ARHCF).

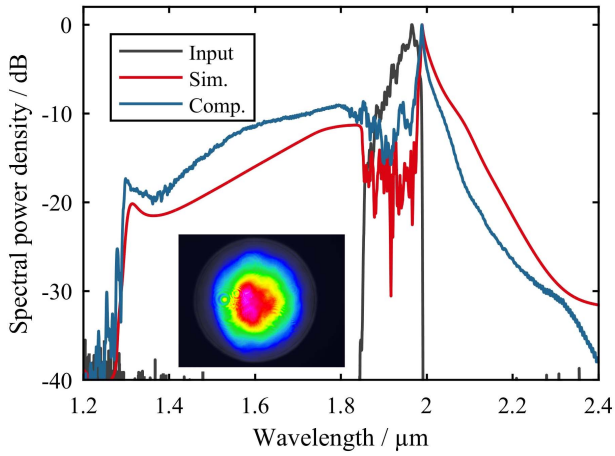


**Fig. 2.** Measured pulse spectra at the NPC stage input (black) and its compressed output (Comp., blue) together with simulation results (Sim., red). Inset: image of the collimated output beam profile.

Our NPC stage consisted of two separate gas-filled pressure chambers that were connected by the ARHCF. The first one, which we denote as the input coupling chamber, was filled with neon gas at a pressure $p_0 = 0.4$ bar. This pressure is a compromise between two opposing requirements. On the one hand, low particle densities, providing a small thermo-optical coefficient, are desirable for the mitigation of thermal blooming, which otherwise reduces the coupling efficiency to the hollow fiber [13]. On the other hand, though, it is important to perform the input coupling in a medium that provides enough thermal conductivity, such that the small but inevitable coupling-losses and the associated heat load close to the fiber tip have no effect on the stability and robustness of the fiber mode excitation at high-average power. As it is known, a higher gas pressure provides a higher thermal conductivity [20]. We successfully found a balanced operation regime that addresses both opposing requirements simultaneously by choosing a light noble gas with a relatively low pressure. The fiber itself was a node-less 7-capillary ARHCF [21,22]. It was fabricated in-house at the University of Central Florida using

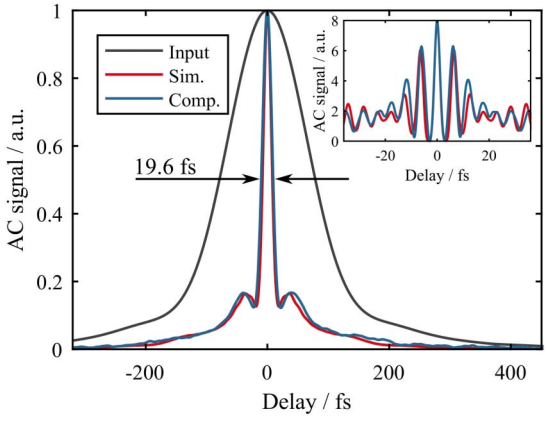


**Fig. 3.** Measured intensity AC traces at the input (black) and compressed output (Comp., blue) of the NPC stage together with simulation results (Sim., red). Inset: interferometric AC measurement (blue) and simulation results (red).

OH-reduced silica glass. A cross-section of the fiber is depicted in Fig. 1. It had an inner core diameter of 53 μm and a core wall thickness of 535 nm. For the experiments presented herein, we used a length of 42 cm. The fiber design provides low-loss broadband transmission, especially at wavelengths spanning from 1.5 μm to 3.0 μm. Consequently, we have achieved >90% transmission through the ARHCF, including coupling losses. The output of the ARHCF was located within a second pressure chamber that was filled with argon gas at a pressure $p_1 = 3$ bar, which is close to the maximum pressure-handling capabilities of the mechanical components in use. In order to circumvent chromatic aberrations and undesired dispersive effects, we used a spherical gold mirror to collimate the light emerging from the fiber output. Before characterization, the shortened pulses went through a 1 mm thick OH-reduced fused silica piece of glass, which served as an output window of the pressure chamber.

In analogy to previously reported experiments [16,23], the pulse evolution along the ARHCF was dominated by the interplay of self-phase-modulation-induced spectral broadening and simultaneous temporal compression due to the anomalous waveguide dispersion. Thus, strong spectral broadening with a 20 dB width of about 800 nm was observed after the NPC stage, as can be seen in Fig. 2 (blue line). The compressed pulse spectrum features a sharp edge at around 1300 nm, which corresponds to the short wavelength boundary of the ARHCF transmission window. Furthermore, Fig. 2 shows that the spectral center of mass was blue-shifted (to about 1820 nm). We found that the reason for this observation was the onset of ionization within the last few cm of the ARHCF, where the pulses are almost fully compressed, leading to a significant spectral blue shift [24]. This behavior and the fact that the spectral guidance of the ARHCF was clamped to >1300 nm caused a slight decrease in the overall transmission to about 84% in high-power operation. The NPC output average power was 43 W, corresponding to 34.4 μJ of pulse energy. An image of the collimated output beam profile showing no sign of thermal blooming at this performance level is depicted in the inset of Fig. 2.

The temporal characterization of the NPC output was performed using two different autocorrelation (AC) techniques. As can be seen in Fig. 3, we have achieved a significant temporal pulse compression of the NPC input (black line) as compared to the compressed output (blue line). The FWHM duration of the intensity AC trace measured after the NPC stage was <20 fs, which indicates a few-cycle pulse duration. In order to confirm this result, we have also performed an interferometric AC measurement using a different autocorrelator. The result of this measurement can be seen in the inset of Fig. 3. The blue curve shows exactly five maxima and, thus, four fringe periods within the FWHM time span of the main temporal feature. The duration of one fringe period corresponds to the duration of the electric field cycle, which is in our case 6.1 fs (as can be calculated from the central wavelength of 1820 nm). As in the case of the intensity AC measurement, an appropriate deconvolution factor has to be found before the FWHM pulse duration or the number of electric field cycles within this time span can be accurately determined.

In order to gain a deeper understanding of the underlying physical processes and to derive the output pulse duration as well as the pulse peak power, we have performed a numerical simulation of the pulse evolution along the NPC stage. In the following, the important features of our simulation tool based on the split-step Fourier method will be summarized. This model describes the pulse evolution in the slowly evolving wave approximation [25], and it includes ionization effects that can cause a sudden change of the temporal nonlinear refractive index across the pulse introduced by the behavior of free carriers, as described by the Drude model [24,26]. The ionization rates are calculated using the Ammosov–Delone–Krainov model [27]. To describe the fiber dispersion across the very broad spectrum, we use the wavelength-dependent refractive index distribution (rather than a Taylor expansion to a few orders), which is approximated based on the capillary model [28]. Additionally, we approximate the ARHCF resonance present at <1300 nm with a super Gaussian absorption band, and we calculate the associated refractive index change according to the Kramers–Kronig relations. Of course, complete knowledge of the spectral refractive index distribution for the fundamental fiber mode requires finite-element simulations, but we believe that the model used in this work describes the experiments very well, especially because of the large core diameter. It reproduces our experimental observations, as can be seen when comparing the measurements (blue line) and the simulation results (red line) in the spectral and temporal domains in Figs. 2 and 3, respectively. The FWHM duration of the simulated intensity AC is 16.3 fs, which is slightly shorter than our measurement. However, because of the good agreement between the simulation and the experiment, it is a safe estimation to use the numerically found AC deconvolution factors and energy content within the main temporal feature to retrieve the pulse duration and peak power obtained in the experiment. Hence, an accurate evaluation of our experimental measurements is not based on an assumption of the pulse profile but on the understanding of the pulse evolution along the ARHCF and its numerical simulation, which provide important information. Following this approach, we have retrieved a FWHM pulse duration of $19.6\ \text{fs}/1.51 = 13.0$ fs from the intensity AC, which corresponds to 2.1 optical cycles. Similarly, the interferometric AC measurement showed four fringe periods within the FWHM duration, which yields $4/1.84 = 2.2$ optical cycles. We believe that the difference in the temporal measurements arises from the slightly different propagation distances through air within our characterization setup. In the simulation result, 60% of the pulse energy is confined within the main temporal feature of the pulse. Hence, we estimated that a pulse peak power of about 1.4 GW was reached in the experiment described herein. Such peak power levels imply that the peak intensity at the end of the fiber was approaching $10^{14}\ \text{W/cm}^2$, which agrees well with the fact that we have clearly observed ionization effects. These effects prevent further spectral broadening and temporal pulse shortening by increasing the nonlinear phase accumulation in our case, because they lead to a breakup of the pulse [29]. We have observed such pulse breakup in both experiment and simulation when the pulse energy or the fiber length was further increased, respectively.

Figure 4 depicts the simulated pulse profile (red line) to provide an impression of the temporal power envelope of the pulses available for subsequent experiments (i.e., after the pulses have left the pressure chamber at the NPC-stage output). The few-cycle pulse is located on top of a weak pedestal, which is inherent to temporal self-compression. In fact, the modulation of this pedestal extending from a delay of 20 fs up to 60 fs after the intense main feature arises from the aforementioned edge of the fiber transmission window and its impact on the spectral phase as governed by the Kramers–Kronig relations. The input

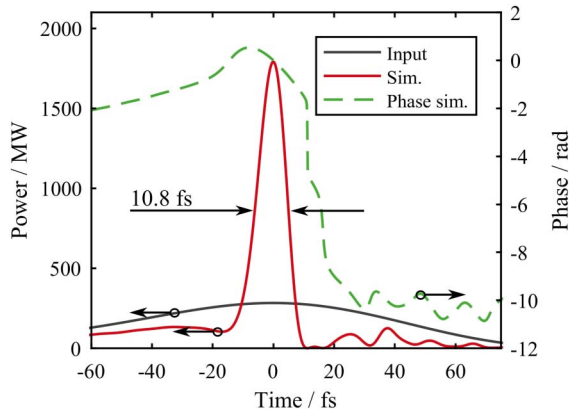


**Fig. 4.** Simulation result of the temporal pulse profile after the NPC stage (Sim., red), together with the simulated temporal phase (Phase sim., green dashed) and a comparison with the input pulse (black).

pulse envelope for the simulation is represented by the black line and shows the significant peak power enhancement after the NPC stage. We have also retrieved the temporal phase from our simulation results, which can be seen in Fig. 4. It is well behaved and almost linearly decreasing across the intense main feature. We found that the pulse duration of our simulated pulse is almost identical to the duration of the transform-limited pulse that can be expected from the measured spectrum.

In conclusion, we have demonstrated a 2.1-cycle laser source with GW-class pulse peak power and a record average power of 43 W spanning the spectral region between 1.3 μm–2.4 μm wavelength. The performance reported in this Letter was enabled by a Tm:FCPA operated at 1.25 MHz repetition rate and a gas-filled ARHCF. The low-loss and broad transmission window of the ARHCF, as well as the fact that the laser system directly provides 110 fs pulses, significantly facilitated the experiments. We have shown that ARHCFs feature excellent power-handling capabilities, which is an important result regarding the immense power-scaling prospects for ultrafast thulium-doped fiber laser systems. The results reported in this work suggest that even shorter pulses approaching the single-cycle regime can be achieved by an optimization of the ARHCF transmission window. Additionally, our findings imply that the next steps will include optimized, larger hollow-core fibers and lighter noble gases at higher pressures, which will allow us to use more pulse energy and to reach even shorter pulse durations, paving the way towards a 100 W-class laser source with sub-2-cycle pulses and mJ-level pulse energy at around 2 μm wavelength.

Aside from these performance-scaling prospects, we have—to the best of our knowledge—demonstrated the highest average power GW-class few-cycle laser source in the 2 μm wavelength region. This source is capable of driving strong-field experiments at high-average power, as tunnel ionization was already observed during the few-cycle pulse generation. Additionally, the achieved GW-class peak power makes this laser source exceptionally interesting for driving broadband intra-pulse DFG with high efficiency and high-average power.

**Funding.** Bundesministerium für Bildung und Forschung (BMBF) (13N13973); Air Force Office of Scientific Research (AFOSR) (FA9550-15-10041); Army Research Office (ARO) (W911NF-12-1-0450).

**Acknowledgment.** F. S. acknowledges support by the Carl-Zeiss Stiftung. M. G. acknowledges support by the Helmholtz-Institute Jena.

## REFERENCES

1. A. Stark, L. Correia, M. Teichmann, S. Salewski, C. Larsen, V. M. Baev, and P. E. Toschek, Opt. Commun. **215**, 113 (2003).
2. K. Scholle, E. Heumann, and G. Huber, Laser Phys. Lett. **1**, 285 (2004).
3. I. Mingareev, N. Gehlich, T. Bonhof, A. Abdulfattah, A. M. Sincore, P. Kadwani, L. Shah, and M. Richardson, Int. J. Adv. Manuf. Technol. **84**, 2567 (2016).
4. S. L. Cousin, F. Silva, S. Teichmann, M. Hemmer, B. Buades, and J. Biegert, Opt. Lett. **39**, 5383 (2014).
5. S. Kazamias, S. Daboussi, O. Guilbaud, K. Cassou, D. Ros, B. Cros, and G. Maynard, Phys. Rev. A **83**, 063405 (2011).
6. F. Silva, S. M. Teichmann, S. L. Cousin, M. Hemmer, and J. Biegert, Nat. Commun. **6**, 6611 (2015).
7. Y. Pertot, C. Schmidt, M. Matthews, A. Chauvet, M. Huppert, V. Svoboda, A. Von Conta, A. Tehlar, D. Baykusheva, J.-P. Wolf, and H. J. Wörner, Science **355**, 264 (2017).
8. I. Pupeza, D. Sánchez, J. Zhang, N. Lilienfein, M. Seidel, N. Karpowicz, T. Paasch-Colberg, I. Znakovskaya, M. Pescher, W. Schweinberger, V. Pervak, E. Fill, O. Pronin, Z. Wei, F. Krausz, A. Apolonski, and J. Biegert, Nat. Photonics **9**, 721 (2015).
9. J. Zhang, K. Mak, N. Nagl, M. Seidel, D. Bauer, D. Sutter, V. Pervak, F. Krausz, and O. Pronin, Light Sci. Appl. (2017) (submitted).
10. Y. Shamir, J. Rothhardt, S. Hädrich, S. Demmler, M. Tschernajew, J. Limpert, and A. Tünnermann, Opt. Lett. **40**, 5546 (2015).
11. K.-H. Hong, S.-W. Huang, J. Moses, X. Fu, C.-J. Lai, G. Cirmi, A. Sell, E. Granados, P. Keathley, and F. X. Kärtner, Opt. Express **19**, 15538 (2011).
12. M. Gebhardt, C. Gaida, S. Hädrich, F. Stutzki, C. Jauregui, J. Limpert, and A. Tünnermann, Opt. Lett. **40**, 2770 (2015).
13. M. Gebhardt, C. Gaida, F. Stutzki, S. Hädrich, C. Jauregui, J. Limpert, and A. Tünnermann, Opt. Lett. **42**, 747 (2017).
14. F. Stutzki, C. Gaida, M. Gebhardt, F. Jansen, A. Wienke, U. Zeitner, F. Fuchs, C. Jauregui, D. Wandt, D. Kracht, J. Limpert, and A. Tünnermann, Opt. Lett. **39**, 4671 (2014).
15. C. Gaida, M. Gebhardt, F. Stutzki, C. Jauregui, J. Limpert, and A. Tünnermann, Opt. Lett. **41**, 4130 (2016).
16. T. Balciunas, C. Fourcade-Dutin, G. Fan, T. Witting, A. A. Voronin, A. M. Zheltikov, F. Gerome, G. G. Paulus, A. Baltuska, and F. Benabid, Nat. Commun. **6**, 6117 (2015).
17. K. Murari, G. J. Stein, H. Cankaya, B. Debord, F. Gérôme, G. Cirmi, O. D. Mücke, P. Li, A. Ruehl, I. Hartl, K.-H. Hong, F. Benabid, and F. X. Kärtner, Optica **3**, 816 (2016).
18. S. D. Jackson and T. King, J. Lightwave Technol. **17**, 948 (1999).
19. M. Gebhardt, C. Gaida, F. Stutzki, S. Hädrich, C. Jauregui, J. Limpert, and A. Tünnermann, Opt. Express **23**, 13776 (2015).
20. V. Antonetti, A. Bar Cohen, A. Bergles, L. Fletcher, J. Howell, J. Johnston, D. A. Kaminski, A. Kraus, F. Kreith, R. Lahey, S. Pantankar, M. Shah, and J. Weisman, *Fluid Flow Databook* (General Electric, Genium Publishing, 1982), Section 410.2, pp. 1–60.
21. W. Belardi and J. C. Knight, Opt. Express **22**, 10091 (2014).
22. F. Yu and J. C. Knight, Opt. Express **21**, 21466 (2013).
23. C. Gaida, M. Gebhardt, F. Stutzki, C. Jauregui, J. Limpert, and A. Tünnermann, Opt. Lett. **40**, 5160 (2015).
24. M. F. Saleh, W. Chang, P. Hölzer, A. Nazarkin, J. C. Travers, N. Y. Joly, P. St.J. Russell, and F. Biancalana, Phys. Rev. Lett. **107**, 203902 (2011).
25. T. Brabec and F. Krausz, Phys. Rev. Lett. **78**, 3282 (1997).
26. W. Chang, A. Nazarkin, J. C. Travers, J. Nold, P. Hölzer, N. Y. Joly, and P. St.J. Russell, Opt. Express **19**, 21018 (2011).
27. M. V. Ammosov, N. B. Delone, and V. P. Krainov, Sov. Phys. JETP **64**, 1191 (1986).
28. J. C. Travers, W. Chang, J. Nold, N. Y. Joly, and P. St.J. Russell, J. Opt. Soc. Am. B **28**, A11 (2011).
29. P. Hölzer, W. Chang, J. C. Travers, A. Nazarkin, J. Nold, N. Y. Joly, M. F. Saleh, F. Biancalana, and P. St.J. Russell, Phys. Rev. Lett. **107**, 203901 (2011).